ORIGINAL ARTICLE

lajss.org Latin American Journal of Solids and Structures

www.lajss.org

Numerical analysis of high-strength concrete columns interconnected by normal-strength concrete floor

Fabio Selleio Prado [a,b]*, Fernando Rebouças Stucchi [a], Leila Cristina Meneghetti [a]

[a] Departamento de Engenharia de Estruturas e Geotécnica, Escola Politécnica, Universidade de São Paulo. Av. Prof. Almeida Prado, trav.2 nº. 83, São Paulo, SP, Brasil. E-mails: fabioselleio@usp.br, fernando.stucchi@poli.usp.br, lmeneghetti@usp.br
[b] Instituto Mauá de Tecnologia, Praça Mauá 01, São Caetano do Sul, SP, Brasil.

* Corresponding author

https://doi.org/10.1590/1679-78256714

Abstract

The construction methods currently adopted for multi-story concrete buildings resorts the strategy to cast columns and slabs with high and normal compressive concrete strength, respectively. The intersection region affects the load transfer performance of the columns, causing expressive confinement stress in interior columns. However, when the confinement is only provided by two sides, as corner columns, it is not enough to increase the lateral stress. The structural behavior of corner columns, represented by isolated columns, also called sandwich column, is investigated in this paper through numerical nonlinear models. The lateral stresses induced by the uniaxial load applied to the sandwich columns are computed when the influence of concrete strength column-slab ratio, slab thickness and the column width ratio and the biggest dimension of the column's cross section were tested. A set of expressions were proposed to calculate the effective compressive strength of the column based on numerical results. The predicted effective strength has shown a good agreement with experimental results collected from the literature.

Keywords

effective compressive strength. Finite Element Method. Reinforced concrete. Confinement. High strength concrete.

Graphical abstract

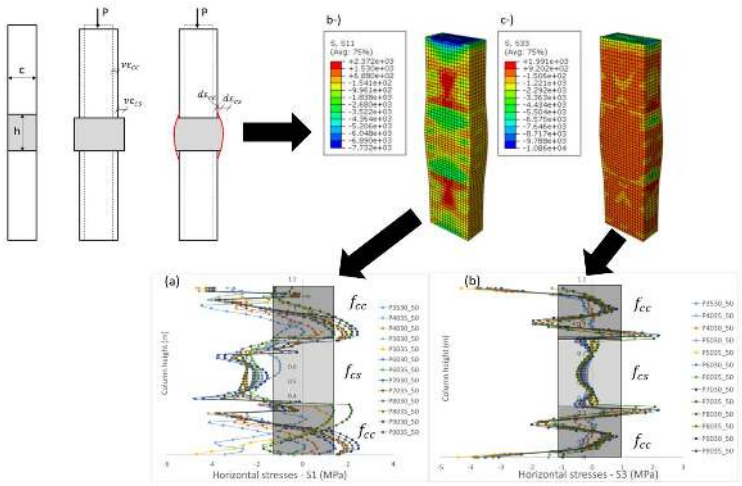

Received August 25, 2021. In revised form October 24, 2021. Accepted October 24, 2021. Available online October 26, 2021
https://doi.org/10.1590/1679-78256714

Latin American Journal of Solids and Structures. ISSN 1679-7825. Copyright © 2021. This is an Open Access article distributed under the terms of the Creative Commons Attribution License, which permits unrestricted use, distribution, and reproduction in any medium, provided the original work is properly cited.

1 INTRODUCTION

The rationed use of materials is a fundamental aspect of civil engineering construction providing efficiency both in structural and economic aspects. The load applied on the columns in multi-story buildings is considerably increased as more floors are added, making it necessary to increase the cross-section of the columns or the strength of concrete. The later solution in which columns are typically cast with high compressive strength (HCS) ranging 60MPa to 120MPa (Guidotti, Ruiz and Muttoni, 2011) and beams or slabs with normal compressive strength (NCS) of 30MPa is widespread structural system. High strength concrete is not required in such elements as beams and slabs, since both are subjected mainly to the bending moment. In this case, the high strength concrete columns are intersected by slabs or beams with normal strength concrete. Thus, the portion of the column made with a lower concrete strength affects the load-transfer performance of the column, creating a column-slab joint with a particular structural behavior. As pointed by Guidotti, Ruiz, and Muttoni (2011), the ultimate limit state of column design will be potentially by slab crushing. However, the structural elements that surround the slab-column joint restrain lateral deformation, generating a confinement of this joint in favor of the concrete strength.

Bianchini et al. (1960) conducted the first experimental research to study the interaction of compressive strength ratio of the columns and slab in different confinement conditions, i.e., interior, edge and corner columns. Based on the results, the authors set up an expression to take into account the reduction induced by the NCS slab in the load transfer performance of HCS columns. This expression was incorporated in the ACI 318-63 with a minor modification and remains the same until ACI 318-19.

Later, Gamble and Klinar (1991); Shu and Hawkins (1992); Kayani (1992); Ospina and Alexander (1998); McHarg et al. (2000); Tula et al. (2000); Freire (2003); Santos (2004); Ali Shah and Ribakov (2005, 2008 and 2011); Caporrino (2007); Meira (2009); Freire (2003); Azevedo (2014); Urban et al. (2015); Shin et al. (2015 e 2017) and Choi et al. (2020) carried out experimental and analytical research to investigate besides the effects of the compressive strength of the column (f_{cc}) and the slab (f_{cs}), others intervenient variables such as the column width (c), the slab thickness (h), the eccentricity of the load on the column and the reinforcement ratio in the beam or slab on the effective compressive strength of the column (f_{cef}). Ali Shah and Ribakov (2011) proposes to calculate the effective strength of the inner columns through the use of a neural network. This way, it is not necessary to use a linear regression of the experimental results, obtaining smaller errors in the prediction of the column strength.

Shu and Hawkins (1992) evidenced the importance of the slab thickness (h) and column size (c) ratio in the load transfer performance of the column, in which the results of experimental tests have shown clearly that smaller is h/c, greater is the effective compressive strength of the column. Some conclusions were also verified by Kayani (1992), Ospina and Alexander (1998), Lee and Mendis (2004), and Caporrino (2007). Ospina and Alexander (1998) have shown that the dimension designed for the rectangular column cross-section should be the smaller one to find the better performance.

Nevertheless, the most variable studied was the location of the column in the structure: interior, edge, or corner of the structure. The experimental results obtained by Bianchini et al. (1960) had not shown substantial increase in the effective compressive strength of edge, corner, and sandwich column. For this reason, they had not proposed any expression for them. Gamble and Klinar (1991) focused their experimental tests on interior and edge columns and based on experimental results, different expressions were proposed for these two location cases. Experimental tests for the sandwich columns, i.e., isolated columns, were made by Shu and Hawkins (1992), Lee and Mendis (2004), Shin et al. (2017) and Choi et al. (2020) whom proposed a different expression to evaluate the effective resistance of the column. Caporrino (2007) proposed a modified expression based on the Gamble and Klinar (1991) for edge and corner columns.

In most of the specimens studied, a square column cross section was studied, although rectangular or circular section can present different results. Tula et al. (2000) tested interior circular cross section column and Ospina and Alexander (1998), Lee and Mendis (2004) and Azevedo (2014) tested the rectangular cross section one, concluding that the smallest dimension of the cross section should be used for the (h/c) ratio.

Shah et al. (2005) and McHarg et al. (2000) had shown the slab reinforcement can provide an increase of the effective compressive strength of the columns. McHarg el al. (2000) additionally indicated that when the slab steel reinforced bars are more concentrated on the column region, higher is the effective compressive strength of the column.

According to the American concrete code ACI 318-19 (2019), if the story concrete strength is greater than 70% of the concrete column strength ($f_{cs} \geq 0{,}7.f_{cc}$), it is not necessary to calculate the reduction in the load transfer performance, allowing to consider the integral column concrete strength for internal, edge and corner location.

If the strength of the pavement concrete is less than 70% of the strength of the column ($f_{cs} < 0{,}7.f_{cc}$), and the four sides of the column are restrained by beams (with the same width as the column) or slabs, the expression presented by the American concrete code ACI 318-19 (2019) can only be used when the column concrete strength is less than 2.5 times the slab concrete strength ($f_{cc} < 2{,}5.f_{cs}$).

$$f_{cef} = 0{,}75.f_{cc} + 0{,}35.f_{cs} \quad (1)$$

The American concrete code ACI 318 (2019) recommends the puddling method for edge or corner columns when $f_{cs} < 0{,}7.f_{cc}$). The Canadian code CSA.A23.3 (2014) expressions are also based on the relation between f_{cc} and f_{cs}, being specific for internal, edge and corner column location, given as follow.

Interior column:

$$f_{cef} = 0{,}25.f_{cc} + 1{,}05.f_{cs} \leq f_{cc} \quad (2)$$

Edge column:

$$f_{cef} = 1{,}4.f_{cs} \leq f_{cc} \quad (3)$$

Corner column:

$$f_{cef} = f_{cs} \quad (4)$$

As pointed by Choi et al. (2020), the effective compressive strength specified in the current design codes (ACI 318-19; CSA A.23.3-14) cannot reflect the effects of the many variables that affect the load transfer performance, beside to provide conservative estimation compared with experimental results for corner columns. Considering that experimental tests are expensive and time consuming, this research aims to investigate the structural behavior of sandwich column through numerical nonlinear models. The lateral stresses were computed considering the influence of the concrete strength column-slab ratio (f_{cc}/f_{cs}), slab thickness and the column width ratio (h/c), and the biggest dimension b of the column's cross section. Based on the numerical experiments results a method to evaluate the effective compressive strength of the sandwich column is proposed.

2 Confinement of the sandwich column

Confinement can be understood as the restriction of lateral strain for a structural element subjected to axial loads. In reinforced concrete, this restriction can be achieved with the application of active pressure contrary to lateral strain or passively employing steel stirrups, wrapping jackets, slabs, and beams or in the case of this work, the higher strength concrete above and below of the conventional strength concrete where the slab or beam would be. As concrete is a frictional material, when subjected to confining stresses, it presents a gain of strength and ductility.

The strength of the confined concrete f_{cc} can be estimated as a function of the confinement stress, σ_{lat} and the strength of the concrete f_c. According to Guidotti et al. (2011), an expression that has shown good results in experimental tests is:

$$f_{cc} = f_c + \alpha_f f_c^{1-\beta_f} {\sigma_{lat}}^{\beta_f} \quad (5)$$

Based on 41 experimental tests, Guidotti et al. (2011) propose that $\alpha_f = 3$ and $\beta_f = 2/3$. However, for confining stresses lower than $0{,}6f_c$, like presented in this study case, a linear approximation as the one proposed by Richart and Brown (1934) in Equation 6 is enough to represent the confinement behavior.

$$f_{cc} = f_c + k\sigma_{lat} \quad (6)$$

If $\alpha_f = 4.1$ and $\beta_f = 1$ are used in Equation (5), it becomes Equation (6) with $k = 4.1$.

In the case of the sandwich column, this confinement stress can mainly vary according to the dimensions of the column, slab thickness, concrete strengths and the steel stirrups. The influence of steel stirrups according to Kayani (1992) does not lead to an increase of the confinement in the joint region, thus the confinement provided by stirrups was neglected in this study. In general, lateral stresses are the confinement stresses in the region of conventional concrete strength like described in Figure 1. Figure 1 (a) shows the sandwich column unloaded. Supposing that the high strength concrete part of the column is not constrained and the normal concrete strength (slab/beam) act independently

when a vertical load is applied, as it is shown in Figure 1 (b), the transverse strain of the column, a function of the Poisson's ratio, is different at each part. The high strength concrete is more rigid than the normal strength concrete than it presents smaller strains ($\upsilon\varepsilon_{cc} < \upsilon\varepsilon_{cs}$). In real sandwich columns, shown in Figure 1 (c), the transverse strains of the sandwich column are constrained between the different concrete strengths. Thus, at the connection of the high strength concrete with the normal strength concrete, there is transverse strain compatibility.

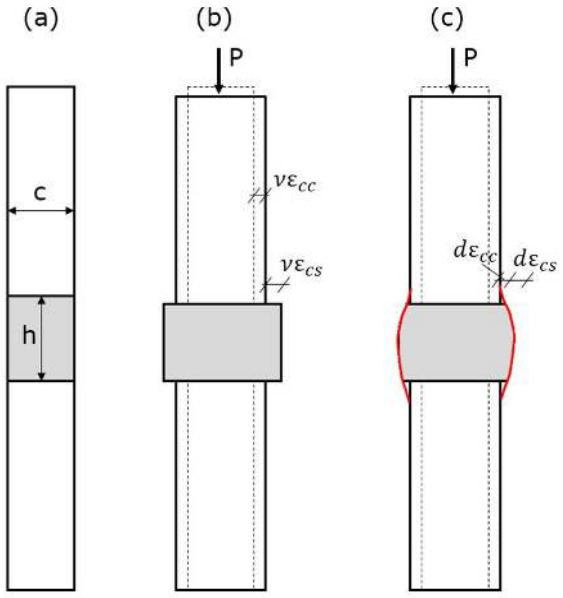

Figure 1 - Distribution of lateral strain along the column.(a) Unloaded column; (b) Loaded column with independent strains; (c) Loaded column considering the compatibility between strains.

Where *P* is the axial load, *c* is the smallest dimension of the column section, *h* is the thickness of the beam/slab, υ is the Poisson's ratio, ε_{cc} is the axial strain of the higher strength concrete (column), ε_{cs} is the axial strain of the conventional strength concrete (slab), $d\varepsilon_{cc}$ and $d\varepsilon_{cs}$ is the lateral strain of the column considering the compatibility between the column and slab concrete.

According to Figure 1 (c), the NSC portion with lower elasticity modulus exhibits greater transverse strain when compared to the HSC which presents larger elasticity modulus. However, due to strain compatibility, the high strength concrete restrains the normal strength concrete. Therefore, the NSC is confined at the connection by the HSC. Consequently, tensile forces appear immediately above the slab-column connection. From the equilibrium of horizontal forces, these tensile forces (T) are balanced by compression forces (C) as shown in Figure 2.

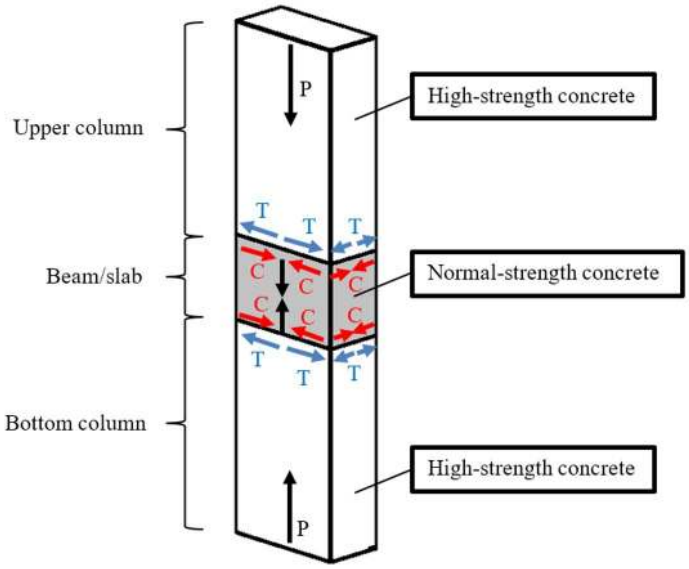

Figure 2 - Distribution of forces along the sandwich column.

The distribution of lateral stresses is shown in Figure 3, which can be assumed parabolic or linear along the NSC slab or beam and HSC column, depending on the h/c ratio and on the shape of the column. It was assumed a lateral stresses distribution like shown in Figure 3a and Figure 3b for higher h/c ratio (h/c >1) and shorter h/c ratio (h/c <1), respectively. For (h/c >1) the restrain given by the high strength concrete it is not sufficient to generate confinement stresses in the middle of the normal strength concrete. Integrating these stresses, the compressive and tensile forces will be found. It is noted that there is not a lateral compressive force along the slab/beam region for higher h/c ratios, only near the connection with the upper and bottom column. Thus, it is expected a minimum increase of resistance of the column in this case. For a shorter h/c ratio (h/c<1), there are compressive lateral forces all along the slab/beam region, therefore this region is confined and may generate an increase of resistance for the column. The red color is for compression force and blue color for tension force.

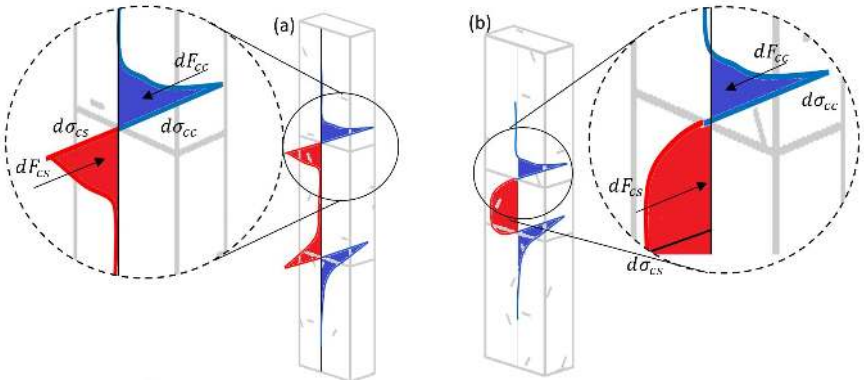

Figure 3 - Distribution of lateral stresses on the column. (a) Higher h/c ratios; (b) Shorter h/c ratios;

The lateral stress on the slab ($d\sigma_{cs}$) and column ($d\sigma_{cc}$) concrete can be calculated through the Hooke's law, using the elastic modulus of the concrete slab and column, E_{cs} and E_{cc}, respectively.

$$d\sigma_{cs} = d\varepsilon_{cs}E_{cs} \tag{7}$$

$$d\sigma_{cc} = d\varepsilon_{cc}E_{cc} \tag{8}$$

Applying the equilibrium of forces presented in Figure 3, the result is :

$$dF_{cc} = dF_{cs} \tag{9}$$

where

$$dF_{cc} = \int d\sigma_{cc}dA = d\varepsilon_{cc}E_{cc}A_{cc} \tag{10}$$

$$dF_{cs} = \int d\sigma_{cs}dA = d\varepsilon_{cs}E_{cs}A_{cs} \tag{11}$$

thus

$$d\varepsilon_{cc}E_{cc}A_{cc} = d\varepsilon_{cs}E_{cs}A_{cs} \tag{12}$$

The area where the lateral stresses is applied on the column is A_{cc} and on the slab is A_{cs}. These areas are very difficult to compute analytically because of their variation according to the column cross-section dimension, slab thickness and concrete strengths ratio. In this paper, we present a new methodology to calculate these areas based on extensive numerical experiments performed.

The strain compatibility equation between the different concrete strengths can be expressed as:

$$d\varepsilon_{cc} + \nu\varepsilon_{cc} = \nu\varepsilon_{cs} - d\varepsilon_{cs} \tag{13}$$

From the equilibrium and the compatibility equations, the horizontal strains and stresses can be determined as follow:

$$d\varepsilon_{cc} = \frac{\nu E_{cs} A_{cs} (\varepsilon_{cs} - \varepsilon_{cc})}{E_{cc} A_{cc} + E_{cs} A_{cs}} \tag{14}$$

$$d\varepsilon_{cj} = \frac{\nu E_{cs} A_{cc} (\varepsilon_{cs} - \varepsilon_{cc})}{E_{cc} A_{cc} + E_{cs} A_{cs}} \tag{15}$$

$$d\sigma_{cc} = \frac{\nu E_{cs} E_{cc} A_{cs} (\varepsilon_{cs} - \varepsilon_{cc})}{E_{cc} A_{cc} + E_{cs} A_{cs}} \tag{16}$$

$$d\sigma_{cs} = \frac{\nu E_{cs} E_{cc} A_{cc} (\varepsilon_{cs} - \varepsilon_{cc})}{E_{cc} A_{cc} + E_{cs} A_{cs}} \tag{17}$$

The Equation 6 was used as a compression failure criterion with the parameter $k = 4.1$ proposed by Richart and Brown (1934).

$$\sigma_{cs,failure} = f_{cs} + 4.1 d\sigma_{cs} - \sigma_i = 0 \tag{18}$$

A tensile concrete failure criterion was not defined because it was assumed that tension will be held by the column stirrup.

To evaluate the lateral confining stress, it is necessary to predict the longitudinal strain of the column, for that, it was used the expression of the Brazilian code ABNT NBR6118 (2014) for the high strength concrete as follow:

$$\varepsilon_{cc} = \varepsilon_{c2} \left(1 - \sqrt[n]{1 - \frac{\sigma_i}{f_{cc}}} \right) \tag{19}$$

A modified expression of the Brazilian code ABNT NBR6118 (2014) was used for the NSC (slab/beam concrete) considering the confinement as follow. The expression used by Choi et al. (2018) did not consider the confinement in this expression, resulting in a lack of convergence in the equilibrium.

$$\varepsilon_{cs} = \varepsilon_{c2} \left(1 - \sqrt[n]{1 - \frac{\sigma_i}{f_{cs} + 4.1 d\sigma_{cs}}} \right) \tag{20}$$

where

$$\varepsilon_{c2} = \begin{cases} 2{,}0\ ‰\ for\ (f_{cc}\ or\ f_{cs}) \leq 50MPa \\ 2{,}0\ ‰ + 0{,}085‰ (f_c - 50)^{0{,}53}\ for\ (f_{cc}\ or\ f_{cs}) > 50MPa \end{cases} \tag{21}$$

$$n = \begin{cases} 2\ for\ (f_{cc}\ or\ f_{cs}) \leq 50MPa \\ 1{,}4 + 23{,}4 \left[\left(\frac{90 - f_c}{100} \right) \right]^4\ for\ (f_{cc}\ or\ f_{cs}) > 50MPa \end{cases} \tag{22}$$

ε_{c2} is the strain at the beginning of the plastic stresses of the concrete.

Choi et al. (2018) used linear elastic finite element models with limited geometric variation to find which length gives the areas A_{cc} and A_{cs}. To improve the results, we have studied several nonlinear finite element models varying the columns dimensions, slab thickness and concrete strengths. These results were validated with the numerical models and with experimental specimens found in the bibliography.

3 Numerical simulations of sandwich columns

Numerical simulations of concrete sandwich columns were developed using ABAQUS software based on the finite element method. The model consists of a rectangular concrete sandwich column in which the top and bottom portion are composed of HSC and the middle is composed of NSC, varying the cross section and height (Figure 4).

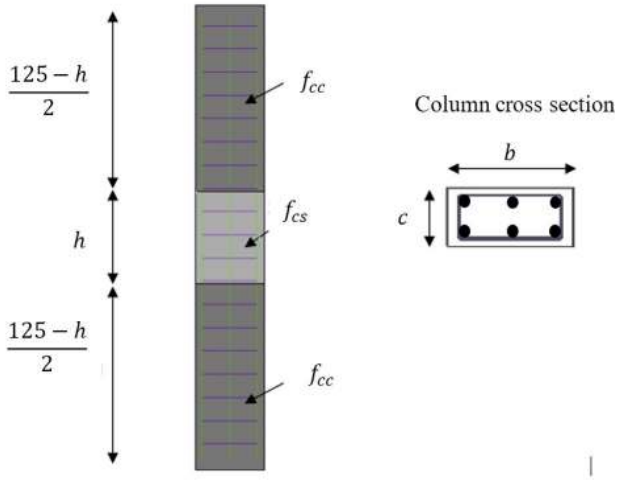

Figure 4 - Sandwich column studied (units: cm).

It was made four major types of numerical models. The Model "R" is the reference model, where the concrete strength of the slab and column are the same and the rectangular column cross-section has the dimensions of 14x30cm. The Model "PS-30" is a rectangular sandwich column with the same dimensions as the reference model, but the concrete strength ratio of the column and the slab range from 1.16 to 3. The slab thickness was varied within the concrete strength ratio, therefore the ratio between the slab thickness and the smallest dimension of the column (h/c) ranges from 0.6 to 5. The Model "PS-45" is a sandwich column with a rectangular cross section of 14x45cm varying the same concrete strength ratios of the model "PS-30". The ratio between the slab thickness and the smallest dimension of the column (h/c) were 0.71 and 3.57. The Model "PS-60" differ from the latter only on the cross-section dimension of the column, which is 14x60cm. Summarizing, the variables studied and their variation are: b from 30 cm to 60 cm; c equal to 14 cm; f_{cc} from 30MPa to 90MPa; f_{cs} from 30MPa to 35 MPa and h from 8.4cm to 70cm. The h/c ratio bigger than 1 is not typical for flat slab buildings, although this study also wishes to include buildings with beams, that will generate greater h/c ratios.

According to the Brazilian concrete code (ABNT NBR 6118: 2014), the bar diameter should not be less than 10mm. In that case, 3 bars on each side of the largest faces of the column were adopted, totalizing 6 bars of 10mm in the cross-section. The construction method of multi-story buildings usually demands the existence of dowels to transfer the forces (lap splice) from the upper column rebar to the bottom column rebar. Considering that these dowels generally are above the slab level, the confinement are unchanged. In the case of the dowels are placed at the slab level, reducing the concrete stresses and its confinement in this place. Thus, for a better confinement behavior of the normal strength concrete, the dowels should be above the slab. Therefore, the dowel effect was neglected in this paper. Stirrups of 6.3 mm diameter each 120 mm were adopted, respecting the minimum reinforcement and spacing recommended, generating the minimum confinement contribution, as the main topic of this paper is the confinement by the high strength concrete.

A 3D model was elaborated using 6615 solid elements with linear function and a single point of integration (C3D8R). Each solid element is a cube with equal sides of 2 cm. It was also used 138 truss elements with linear function to represent the steel reinforcement bars (T3D2). Figure 5 shows the model simulated. Furthermore, in this model, steel and concrete were simulated considering nonlinear behavior through their plasticity.

A reference point has been created at the top end of the column to apply the loading. This reference point was coupled to the upper nodes of the column using a Multiple Point Constraint (MPC). In the vertical direction was added a displacement, incremented over the processing time in a linear mode, starting from zero to 3mm. It was considered that the steel bars are immersed in the concrete with an embedded interface, simulating the reinforced concrete behavior. No slip law was considered because this effect was not found in the experimental studies by previous researchers, as for example Bianchini et al. (1960), Shu and Hawkins (1992), Ospina and Alexander (1998), Shin et al. (2015 e 2017) and Choi et al. (2020).

The initial time increment for the Newton-Raphson solution was 10^{-5} and the minimum time increment required was 10^{-6}. These very small steps contribute to the model's convergence.

It is important to choose correctly the most suitable constitutive model to represent the complex nonlinear behavior of the concrete. While most engineering problems can be treated as a typical two-dimensional (plane) stress states, the confined column is a triple stress state, since the transversal strain and its effect also have to be considered in both directions for a rectangular cross section column, for example.

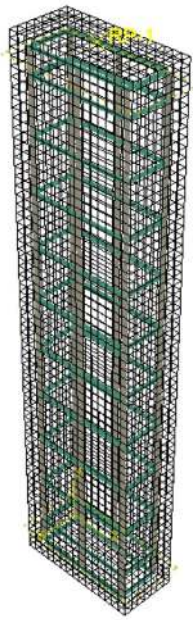

Figure 5 - Finite element model used for the analysis.

According to Maekawa, Pimanmas, and Okamura (2004), the triaxial elasto-plastic state of stresses and the fracture mechanics models should be used before the cracks are generated. These concepts will consider the plastic deformation of reinforced concrete and the loss of the ability to absorb elastic energy due to the damage. The effect of the confinement will be automatically considered by these concepts.

In this paper, it was used the Concrete Damage Plasticity (CDP) criterion to represent the nonlinear behavior of the concrete and its confinement effect on the sandwich columns. This resistance criterion is default in the ABAQUS software and do not need to be implemented, but it should be validated with experimental tests.

3.1 Concrete damage plasticity (CDP) model

The concrete damage plasticity (CDP) model is available in ABAQUS V6.14 and it is an extension created by Lubliner et al. (1989) and Lee and Fenves (1998) from the resistance criterion of Drucker and Prager (1952). This extension allows that the meridians could be curved lines, more precisely hyperbolas, then, the flow surface in the anti-spherical plane might not be circular, governed by the parameter K_c, and those non-associative flow laws could be used.

According to Alfarah et al. (2017), this criterion can be considered the best one representing the complex inelastic concrete behavior, using concepts of isotropic elastic damage in combination with isotropic plasticity in tension and compression.

It can be seen that the CDP depends in four parameters to represent the concrete, being (K_c, ψ, f_{b0}/f_{c0} e ϵ). The parameter K_c is interpreted as a ratio of the distances between the hydrostatic axis and the tension meridian by the hydrostatic axis and the compression meridian in the anti-spherical cross-section. The parameter K_c is given by:

$$K_c = \frac{(\sqrt{J_2})_{TM}}{(\sqrt{J_2})_{CM}} \tag{23}$$

Where $\left(\sqrt{J_2}\right)_{TM}$ is the square root of the second invariant of the anti-spherical part of the tension tensor in the tension meridian; $\left(\sqrt{J_2}\right)_{CM}$ is the square root of the second invariant of the anti-spherical part of the stress tensor in the compression meridian.

This ratio is always greater than 0.5 and, when it assumes a value of 1, the deviatoric cross section of the failure surface becomes a circle (as in the classic hypothesis of Drucker and Prager, 1952). Kaminski and Kmiecik (2011) and in the ABAQUS user's manual (2014) recommend $K_c = 2/3$.

The eccentricity of the flow potential ϵ is a small numerical parameter that defines the rate at which the hyperbolic flow potential approaches its asymptote. In other words, it is the distance between the vertex of the hyperbola and the intersection of the asymptotes of that hyperbola with the abscissa. The eccentricity of the parameters can be calculated

as a ratio between the tensile strength and compressive strength. Kaminski and Kmiecik (2011) and ABAQUS user's manual (2014) recommend $\epsilon = 0.1$, this value helps to achieve faster numerical convergence. When $\epsilon = 0$, the flow potential becomes a straight line, which is the classical Drucker-Prager hypothesis.

Another parameter that describes the state of the material is the rupture of the concrete under biaxial compression, with (f_{b0}/f_{c0}) being the resistance in the biaxial state and the resistance in the uniaxial state ratio. After the approximation with the elliptical equation, the uniform biaxial compression strength f_{b0} is equal to 1,16248 f_{c0}.

The last parameter characterizing the performance of the concrete in a multiaxial stress state is the dilation angle (ψ). The angle is correlated with the increase in inelastic volume due to the increase in anti-spherical stresses, or in relation to the distortion.

Considering that the resistance criterion with a hyperbolic meridional curve is associative, physically the angle of friction will be equal to the angle of dilation. According to Kaminski and Kmiecik (2011) and Malm (2009), usually in simulations $\beta = \psi$ = 30° to 40° is assumed.

As the concrete has a softening behavior and a loss of stiffness that can lead the numerical models to have great difficulties in convergence, a visco-plastic regularization technique was added to the CDP, to allow the stresses exceed the limit of the material flow surface. For this, the viscosity parameter μ must be different of zero. It is recommended that this value be as small as possible so that there is no interference with the results.

3.2 Concrete damage model

A concrete damaged model was considered for both compression and tension behavior.

The evolution of the compressive damage (d_c) is directly related to the plastic strain. According to Birtel et al. (2006) the plastic strain is determined dependent to the inelastic strain (ε_c^{in}) using a constant variable b_c which varies between 0 and 1. The inelastic strain (ε_c^{in}) and the cracking strain (ε_t^{ck}) are defined as the total strain minus the elastic strain corresponding to the undamaged material. The compression damaged expression is:

$$d_c = 1 - \frac{\sigma_c E_0^{-1}}{\varepsilon_c^{pl}(1/b_c - 1) + \sigma_c E_0^{-1}} \tag{24}$$

The plastic strain in compression can be evaluated by the following expression:

$$\varepsilon_c^{pl} = \varepsilon_c^{in} - \frac{d_c}{(1-d_c)} \frac{\sigma_c}{E_0} \tag{25}$$

The damage expression in tension (d_t) is similar to the compression in which the plastic deformation depends on an experimentally parameter b_t varying between 0 and 1 (Birtel et al., 2006) and is dependent to the cracking strain (ε_t^{ck}). The tension damaged expression is:

$$d_t = 1 - \frac{\sigma_t E_0^{-1}}{\varepsilon_t^{pl}(1/b_t - 1) + \sigma_t E_0^{-1}} \tag{26}$$

The plastic strain in tension can be evaluated by the following expression:

$$\varepsilon_t^{pl} = \varepsilon_t^{ck} - \frac{d_t}{(1-d_t)} \frac{\sigma_t}{E_0} \tag{27}$$

Where the σ_c and σ_t are the compression and tension stresses, respectively, and E_0 is the elastic modulus of the concrete.

In this paper the parameters b_c and b_t were adopted as 0.7 and 0.1, respectively, experimentally determined in cyclic compressive and tensile loading by Birtel et al. (2006). Although it was not used cyclic loads in this paper, the damage is important to evaluate where the compressive damage starts on the column and where is the final failure.

3.3 Concrete stress-strain curves

In addition to adopting the parameters for the CDP model listed before (item 3.1) to represent the plastic behavior of concrete, its stress-strain curve is also defined for a uniaxial test for different concrete strengths. The stress-strain curve adopted is that suggested by the fib Model Code 2010 (2013) as following. The curves plotted for several concrete strengths are shown in Figure 6.

$$\sigma_c = f_{cm}\left(\frac{k.\eta-\eta^2}{1+(k-2).\eta}\right) for\ |\varepsilon_c| < |\varepsilon_{c,lim}| \quad (28)$$

Where:

$\eta = \varepsilon_c/\varepsilon_{c1}$;

$k = E_{ci}/E_{c1}$;

σ_c is the compressive stress of the concrete;

ε_{c1} is the strain at maximum compressive stress;

ε_c is the strain for a compressive stress;

E_{c1} is the secant modulus from the origin to the peak compressive stress;

E_{ci} is the tangent modulus from the origin;

$\varepsilon_{c,lim}$ is the limit strain at the concrete;

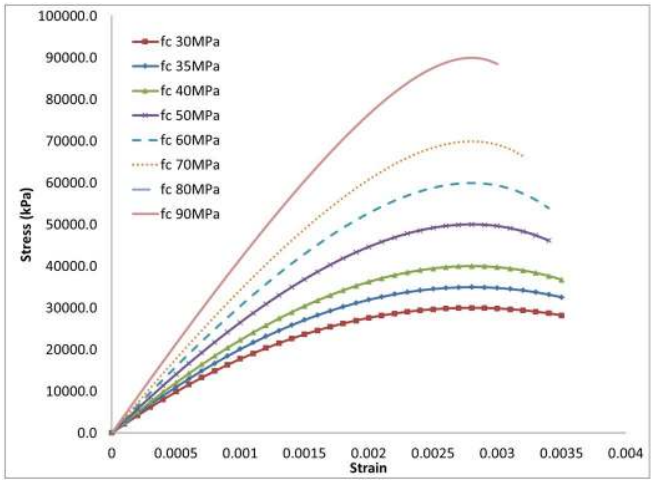

Figure 6 - Compression stress-strain curve by Model Code 2010.

The tensile stress-strain curves, presented on Figure 7, were constructed using the bilinear curve, for $\varepsilon_t \leq \varepsilon_{cr}$ according to ABNT NBR 6118 (2014).

$$\begin{cases} \sigma_t = E_c\varepsilon_t\ for\ \sigma_t < 0.9\ f_{ctm} \\ \sigma_t = f_{ctm}\ for\ \varepsilon_{cr} = 0.15\ ‰ \end{cases} \quad (29)$$

When the $\varepsilon_t > \varepsilon_{cr}$, the relationship proposed by Hsu and Zhang (1996) was applied.

$$\sigma_t = f_{ctm}\left(\frac{\varepsilon_{cr}}{\varepsilon_t}\right)^{0.4} for\ \varepsilon_t > 0.15\ ‰ \quad (30)$$

Where:

- ε_t = elongation strain
- ε_{cr} = crack formation strain = 0.15 ‰
- f_{ctm} = crack formation stress = $\begin{cases} 0.3{f_{ck}}^{2/3}\ for\ f_{ck} \leq 50MPa \\ 2.12\ ln(1+0.11\ f_{ck})\ for\ f_{ck} > 50MPa \end{cases}$

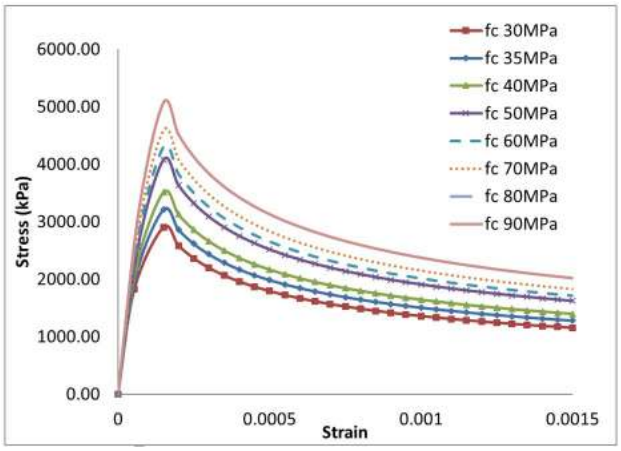

Figure 7 - Tension -stress-strain curve by Model Code 2010.

According to the fib Model Code 2010 (2013) the Poisson's ratio of the concrete is 0.2, which was assumed for all numerical models.

3.4 Steel stress-strain curves

Elastoplastic behavior was assumed for the steel rebar and the ABNT NBR 6118 (2014) was used as basis to construct the stress-strain curve. The reinforced steel bars considered are the CA-50 type, having a yield stress at 500 MPa and a Young Modulus of 210GPa. The stress-strain curve for CA-50 steel bars is shown in Figure 8.

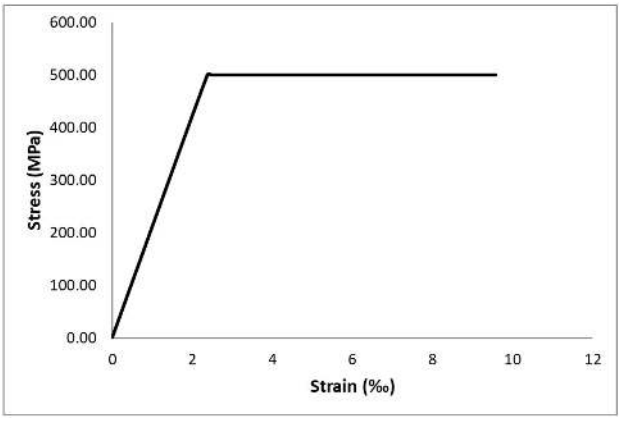

Figure 8 - Stress-strain curve for the steel CA-50.

3.5 Plasticity parameters certification

Experimental results reported by Shu and Hawkins (1992) and Shin et al. (2015) were used to validate the setup parameters in the numerical models. It was an essential step to certify if the numeric model developed accurately represents an experimental column test.

Shu and Hawkings were the first to investigate sandwich column experimentally. The authors investigated the influence of h/c and the column-slab concrete strength ratio. Shin et al. (2015) carried out tests on sandwich columns varying the concrete strength of the slab and column. In the slab the concrete strength varied between 50MPa and 140MPa and in the column strength was 100MPa and 200MPa. The reinforcement area and cross-section dimensions were kept constant. The data of the experimental specimens chosen for the certification are presented in Table 1.

Nonlinear numerical models identical to the experimental were developed in ABAQUS V6.14 using the CDP Model to represent the concrete. The setup CDP Model parameters suggested by Kaminski and Kmiecik (2011) were validated comparing the experimental x numerical results. The final setup parameters used in the numerical experiments using the CDP and their results are shown in Table 2.

Table 1 - Data of experimental tests of Shu and Hawkins (1992) and Shin et al. (2015).

Author	Model ID (EXPERIMENTAL)	f_{cc} (MPa)	f_{cs} (MPa)	f_{cc}/f_{cs}	b (cm)	c (cm)	h (cm)	$P_{rup,\,exp}$ (kN)
Shin et al. (2015)	PS10050	130.7	50.8	2.57	22	22	13.2	**3296.1**
	PS20050	200	50.8	3.94				**3299**
	PS200100	200	130.7	1.53				**6540.9**
	PS200140	200	161	1.24				**7651.1**
Shu and Hawkins (1992)	PS4731	47.57	31.44	1.51	15.24	15.24	30.48	**909.66**
	PS5024	50.81	23.65	2.15			15.24	**845.16**
	PS4818	48.47	18	2.69			7.62	**911.88**

Table 2 - Finite element model data.

Author	Model ID (ABAQUS)	K_c	f_{b0}/f_{c0}	β	μ	Element size (mm)	Element type	$P_{rup,\,ABAQUS}$ (kN)	f_{cef} (MPa)	f_{cef}/f_{cs}
Shin et al. (2015)	PS10050A	0.667	1.16	36°	5E-04	20	C3D8R	**3216.5**	59.2	1.16
	PS20050A							**3216.5**	59.2	1.16
	PS200100A							**6684.8**	132.0	1.01
	PS200140A							**8401.8**	168.1	1.04
Shu and Hawkins (1992)	PS4731A	0.667	1.16	36°	5E-04	20	C3D8R	**911.4**	33.5	1.07
	PS5024A							**781.9**	27.9	1.18
	PS4818A							**776.3**	27.6	1.54

The effective column stress was calculated using the expression proposed in the American Concrete Code ACI 318-19 (2019) as follows:

$$f_{cef} = \frac{P_{rup} - f_y . A_s}{\alpha . (A_g - A_s)} \tag{31}$$

Where f_{cef} is the effective stress on the column; $P_{rup,ABAQUS}$ is the rupture load found on the numerical models;

$P_{rup,exp}$ is the rupture load found on the experimental specimens. f_y is the yield strength of the steel reinforcement bars; A_s is the area of the column longitudinal steel reinforcement bars; A_g is the gross cross-section area of the column; α is a parameter to account for accidental eccentricity recommended to be 0.85 by ACI 318-19 (2019). The parameter α was taken equal to 1 as the accidental eccentricity does not exist in the numerical models.

The numerical results obtained show a good agreement with the experimental ones (see Table 3).

Table 3 - Comparison of numerical and experimental results.

P_{rup} (kN) (ABAQUS)	P_{rup} (kN) (EXPERIMENTAL)	$P_{ABAQUS}/P_{EXPERIMENTAL}$
3216.5	3296.1	1.02
3216.5	3299	1.03
6684.77	6540.9	0.98
8401.79	7651.1	0.91
911.425	909.66	1.00
781.888	845.16	1.08
776.267	911.88	1.17

The average of the difference between experimental and numerical results was 3% and the variance was 1%. Considering that there is natural variability in the concrete composition transferred to the experimental results, this difference is insignificant. It means that the numerical model represents the experimental specimen and can be used to extrapolate to other column dimensions and concrete strength ratios.

3.6 Results

The numerical experiment results in terms of the rupture load, uniaxial compressive stress, effective stress and effective stress-lower strength ratio are summarized in Table 4. The effective compressive strength (f_{cef}) of the numerical models was calculated according the expression given in Eq. 34.

The rupture load was determined by the load vs processing time graph, where it was analyzed which was the peak load.

Table 4 - Results of the numerical experiments.

Model ID (ABAQUS)		Concrete (MPa)		f_{cc}/f_{cs}	Column		Slab thickness	h/c	P_{rup} (kN)	f_{cef} (MPa)	f_{cef}/f_{cs}
		f_{cc}	f_{cs}		b (cm)	c (cm)	h (cm)				
R	PS3030	30	30	1	14	30	-	-	1489.88	30.10	1.00
	PS3535	35	35				-	-	1718.62	35.61	1.02
	PS4040	40	40				-	-	1928.63	40.67	1.02
	PS5050	50	50				-	-	2349.17	50.80	1.02
	PS6060	60	60				-	-	2740.07	60.21	1.00
	PS7070	70	70				-	-	3080.76	68.42	0.98
	PS8080	80	80				-	-	3430.78	76.85	0.96
	PS9090	90	90				-	-	3778.26	85.22	0.95
PS-30	PS3530	35	30	1.17	14	30	70	5.00	1459.89	29.38	0.98
	PS4030	40	30	1.33					1461.11	29.41	0.98
	PS4035	40	35	1.14					1668.03	34.39	0.98
	PS5030	50	30	1.67					1468.66	29.59	0.99
	PS5035	50	35	1.43					1647.91	33.91	0.97
	PS6030	60	30	2.00					1468.74	29.59	0.99
	PS6035	60	35	1.71					1673.71	34.53	0.99
	PS7030	70	30	2.33					1468.56	29.59	0.99
	PS7035	70	35	2.00					1673.14	34.52	0.99
	PS8030	80	30	2.67					1463.55	29.47	0.98
	PS8035	80	35	2.29					1674.37	34.55	0.99
	PS9030	90	30	3.00					1469.44	29.61	0.99
	PS9035	90	35	2.57					1674.87	34.56	0.99
PS-30	PS3530	35	30	1.17	14	30	60	4.29	1471.14	29.65	0.99
	PS4030	40	30	1.33					1479.30	29.85	0.99
	PS4035	40	35	1.14					1678.46	34.64	0.99
	PS5030	50	30	1.67					1484.44	29.97	1.00
	PS5035	50	35	1.43					1689.64	34.91	1.00
	PS6030	60	30	2.00					1484.56	29.97	1.00
	PS6035	60	35	1.71					1686.33	34.83	1.00
	PS7030	70	30	2.33					1488.00	30.06	1.00
	PS7035	70	35	2.00					1693.31	35.00	1.00
	PS8030	80	30	2.67					1490.12	30.11	1.00
	PS8035	80	35	2.29					1688.62	34.89	1.00
	PS9030	90	30	3.00					1489.58	30.10	1.00
	PS9035	90	35	2.57					1698.89	35.14	1.00
PS-30	PS3530	35	30	1.17	14	30	50	3.57	1511.33	30.62	1.02
	PS4030	40	30	1.33					1515.79	30.73	1.02
	PS4035	40	35	1.14					1757.73	36.55	1.04
	PS5030	50	30	1.67					1517.59	30.77	1.03
	PS5035	50	35	1.43					1757.73	36.55	1.04
	PS6030	60	30	2.00					1517.56	30.77	1.03
	PS6035	60	35	1.71					1764.69	36.72	1.05

Table 4 - Continued...

Model ID (ABAQUS)		Concrete (MPa)		f_{cc}/f_{cs}	Column		Slab thickness	h/c	$P_{rup}\ (kN)$	$f_{cef}\ (MPa)$	f_{cef}/f_{cs}
		f_{cc}	f_{cs}		b (cm)	c (cm)	$h\ (cm)$				
	PS7030	70	30	2.33					1535.96	31.21	1.04
	PS7035	70	35	2.00					1752.95	36.44	1.04
	PS8030	80	30	2.67					1537.59	31.25	1.04
	PS8035	80	35	2.29					1753.25	36.45	1.04
	PS9030	90	30	3.00					1539.83	31.31	1.04
	PS9035	90	35	2.57					1769.24	36.83	1.05
PS-30	PS3530	35	30	1.17	14	30	40	2.86	1490.91	30.13	1.00
	PS4030	40	30	1.33					1478.88	29.84	0.99
	PS4035	40	35	1.14					1700.51	35.18	1.01
	PS5030	50	30	1.67					1506.69	30.51	1.02
	PS5035	50	35	1.43					1743.52	36.21	1.03
	PS6030	6 0	30	2.00					1481.62	29.90	1.00
	PS6035	60	35	1.71					1715.55	35.54	1.02
	PS7030	70	30	2.33					1544.26	31.41	1.05
	PS7035	70	35	2.00					1755.46	36.50	1.04
	PS8030	80	30	2.67					1548.14	31.51	1.05
	PS8035	80	35	2.29					1759.71	36.60	1.05
	PS9030	90	30	3.00					1540.30	31.32	1.04
	PS9035	90	35	2.57					1753.31	36.45	1.04
PS-30	PS3530	35	30	1.17	14	30	30	2.14	1505.81	30.49	1.02
	PS4030	40	30	1.33					1540.92	31.33	1.04
	PS4035	40	35	1.14					1720.13	35.65	1.02
	PS5030	50	30	1.67					1541.37	31.34	1.04
	PS5035	50	35	1.43					1799.70	37.57	1.07
	PS6030	60	30	2.00					1556.51	31.71	1.06
	PS6035	60	35	1.71					1754.13	36.47	1.04
	PS7030	70	30	2.33					1564.74	31.91	1.06
	PS7035	70	35	2.00					1784.45	37.20	1.06
	PS8030	80	30	2.67					1563.39	31.87	1.06
	PS8035	80	35	2.29					1780.85	37.11	1.06
	PS9030	90	30	3.00					1588.69	32.48	1.08
	PS9035	90	35	2.57					1808.41	37.77	1.08
PS-30	PS3530	35	30	1.17	14	30	20	1.43	1537.39	31.25	1.04
	PS4030	40	30	1.33					1543.28	31.39	1.05
	PS4035	40	35	1.14					1750.54	36.38	1.04
	PS5030	50	30	1.67					1588.94	32.49	1.08
	PS5035	50	35	1.43					1818.26	38.01	1.09
	PS6030	60	30	2.00					1570.51	32.05	1.07
	PS6035	60	35	1.71					1806.62	37.73	1.08
	PS7030	70	30	2.33					1604.61	32.87	1.10
	PS7035	70	35	2.00					1819.02	38.03	1.09
	PS8030	80	30	2.67					1618.88	33.21	1.11
	PS8035	80	35	2.29					1832.76	38.36	1.10
	PS9030	90	30	3.00					1619.75	33.23	1.11
	PS9035	90	35	2.57					1824.21	38.16	1.09
PS-30	PS3530	35	30	1.17	14	30	14	1.00	1584.94	32.39	1.08
	PS4030	40	30	1.33					1640.84	33.74	1.12
	PS4035	40	35	1.14					1799.85	37.57	1.07
	PS5030	50	30	1.67					1710.38	35.41	1.18
	PS5035	50	35	1.43					1888.38	39.70	1.13
	PS6030	60	30	2.00					1724.38	35.75	1.19
	PS6035	60	35	1.71					1933.52	40.79	1.17

Table 4 - Continued...

Model ID (ABAQUS)		Concrete (MPa)		f_{cc}/f_{cs}	Column		Slab thickness	h/c	$P_{rup}\ (kN)$	$f_{cef}\ (MPa)$	f_{cef}/f_{cs}
		f_{cc}	f_{cs}		b (cm)	c (cm)	$h\ (cm)$				
	PS7030	70	30	2.33					1746.13	36.27	1.21
	PS7035	70	35	2.00					1942.79	41.01	1.17
	PS8030	80	30	2.67					1755.22	36.49	1.22
	PS8035	80	35	2.29					1967.38	41.60	1.19
	PS9030	90	30	3.00					1743.37	36.21	1.21
	PS9035	90	35	2.57					1990.85	42.17	1.20
PS-30	PS3530	35	30	1.17	14	30	10	0.71	1602.36	32.81	1.09
	PS4030	40	30	1.33					1696.08	35.07	1.17
	PS4035	40	35	1.14					1812.87	37.88	1.08
	PS5030	50	30	1.67					1816.51	37.97	1.27
	PS5035	50	35	1.43					1981.21	41.94	1.20
	PS6030	60	30	2.00					1852.40	38.83	1.29
	PS6035	6 0	35	1.71					2018.14	42.83	1.22
	PS7030	70	30	2.33					1904.59	40.09	1.34
	PS7035	70	35	2.00					2085.80	44.46	1.27
	PS8030	80	30	2.67					1957.29	41.36	1.38
	PS8035	80	35	2.29					2141.98	45.81	1.31
	PS9030	90	30	3.00					1998.61	42.36	1.41
	PS9035	90	35	2.57					2185.51	46.86	1.34
PS-30	PS3530	35	30	1.17	14	30	8.4	0.60	1613.57	33.08	1.10
	PS4030	40	30	1.33					1717.46	35.58	1.19
	PS4035	40	35	1.14					1820.19	38.06	1.09
	PS5030	50	30	1.67					1867.00	39.19	1.31
	PS5035	50	35	1.43					2015.20	42.76	1.22
	PS6030	60	30	2.00					1932.12	40.75	1.36
	PS6035	60	35	1.71					2088.18	44.51	1.27
	PS7030	70	30	2.33					1986.79	42.07	1.40
	PS7035	70	35	2.00					2149.22	45.98	1.31
	PS8030	80	30	2.67					2047.23	43.53	1.45
	PS8035	80	35	2.29					2211.19	47.48	1.36
	PS9030	90	30	3.00					2109.62	45.03	1.50
	PS9035	90	35	2.57					2269.87	48.89	1.40
PS-45	PS3530	35	30	1.17	14	45	50	3.57	2332.63	31.67	1.06
	PS4030	40	30	1.33					2341.60	31.82	1.06
	PS4035	40	35	1.14					2644.93	36.69	1.05
	PS5030	50	30	1.67					2356.43	32.06	1.07
	PS5035	50	35	1.43					2671.12	37.11	1.06
	PS6030	60	30	2.00					2356.02	32.05	1.07
	PS6035	60	35	1.71					2662.68	36.97	1.06
	PS7030	70	30	2.33					2363.02	32.16	1.07
	PS7035	70	35	2.00					2677.40	37.21	1.06
	PS8030	80	30	2.67					2366.62	32.22	1.07
	PS8035	80	35	2.29					2679.74	37.25	1.06
	PS9030	90	30	3.00					2372.77	32.32	1.08
	PS9035	90	35	2.57					2683.40	37.31	1.07
PS-45	PS3530	35	30	1.17	14	45	10	0.71	2514.86	34.60	1.15
	PS4030	40	30	1.33					2664.62	37.00	1.23
	PS4035	40	35	1.14					2833.42	39.71	1.13
	PS5030	50	30	1.67					2859.72	40.14	1.34
	PS5035	50	35	1.43					3093.30	43.89	1.25
	PS6030	60	30	2.00					2938.03	41.39	1.38
	PS6035	60	35	1.71					3189.94	45.44	1.30
	PS7030	70	30	2.33					2983.16	42.12	1.40

Table 4 - Continued...

Model ID (ABAQUS)		Concrete (MPa)		f_{cc}/f_{cs}	Column		Slab thickness	h/c	P_{rup} (kN)	f_{cef} (MPa)	f_{cef}/f_{cs}
		f_{cc}	f_{cs}		b (cm)	c (cm)	h (cm)				
	PS7035	70	35	2.00					3249.01	46.39	1.33
	PS8030	80	30	2.67					3066.76	43.46	1.45
	PS8035	80	35	2.29					3335.04	47.77	1.36
	PS9030	90	30	3.00					3141.44	44.66	1.49
	PS9035	90	35	2.57					3412.36	49.01	1.40
PS-60	PS3530	35	30	1.17	14	60	50	3.57	2917.62	32.06	1.07
	PS4030	40	30	1.33					2933.57	32.25	1.08
	PS4035	40	35	1.14					3342.89	37.15	1.06
	PS5030	50	30	1.67					2963.84	32.61	1.09
	PS5035	50	35	1.43					3378.67	37.58	1.07
	PS6030	60	30	2.00					2963.77	32.61	1.09
	PS6035	60	35	1.71					3381.87	37.62	1.07
	PS7030	70	30	2.33					2974.04	32.74	1.09
	PS7035	70	35	2.00					3389.85	37.71	1.08
	PS8030	80	30	2.67					2984.46	32.86	1.10
	PS8035	80	35	2.29					3398.57	37.82	1.08
	PS9030	90	30	3.00					2992.13	32.95	1.10
	PS9035	90	35	2.57					3415.32	38.02	1.09
PS-60	PS3530	35	30	1.17	14	60	10	0.71	3159.65	34.96	1.17
	PS4030	40	30	1.33					3374.37	37.53	1.25
	PS4035	40	35	1.14					3585.78	40.06	1.14
	PS5030	50	30	1.67					3652.21	40.86	1.36
	PS5035	50	35	1.43					3959.97	44.54	1.27
	PS6030	60	30	2.00					3773.13	42.30	1.41
	PS6035	60	35	1.71					4105.73	46.29	1.32
	PS7030	70	30	2.33					3852.49	43.25	1.44
	PS7035	70	35	2.00					4199.33	47.41	1.35
	PS8030	80	30	2.67					3965.55	44.61	1.49
	PS8035	80	35	2.29					4325.36	48.91	1.40
	PS9030	90	30	3.00					4072.72	45.89	1.53
	PS9035	90	35	2.57					4439.33	50.28	1.44

The reference model (Model R) had good agreement with the expected values for the concrete strength below 70MPa. Above this strength, there was a difference of about 5% between the numerical and expected results. As higher is the strength of the concrete more fragile it is and this could generate the difference in the results. However, this difference is insignificant on these analyses.

The effective compressive strength found in the columns with h/c ratio larger than 4 was equal to f_{cs}, evidencing the behavior of the lateral stresses predicted on Figure 3a, where the confinement does not exist in the middle of the column. However, the effective compressive strength was increased to a maximum of 10% when the h/c ratio varied between 1.43 and 3.57. More significant confinement stresses were found for h/c ratio under 1.43. The effective compressive stress was raised in 53% in the Model ID PS-60 - PS9030 – $h/c = 0.714$.

Analyzing the effect of changing the largest dimension of the concrete cross section from 45cm to 60cm, it was observed a small enhance in the effective compressive strength, ranging from 2% to 8%.

The concrete strength ratio proved to be an important factor on the effective resistance of the column. Higher was the concrete strength ratio, higher was the confinement stress; in other words, higher was the effective resistance. It was noted that for equal concrete strengths ratios (f_{cc}/f_{cs}) the effective resistance ratio (f_{cef}/f_{cs}) is also approximately equal. Therefore, the concrete strength ratio is more significant for the f_{cef}/f_{cs} ratio than the concrete strength itself.

As there are many graphical results, it was chosen the results of the column with Model ID PS-30 - PS6030 – $h/c = 3.57$. It is presented on Figure 9 the increase of load versus time until failure, where can been observed that the peak load was approximately at 0.7s and the numerical model will present post peak behavior.

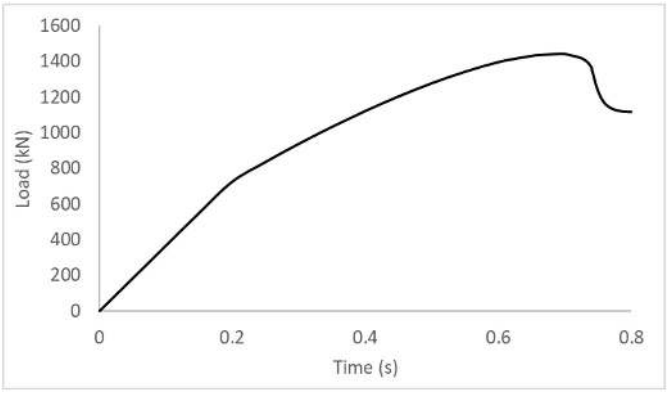

Figure 9 - The numerical model load curve.

All the results presented next are for the maximum load presented on Figure 9, that occurred at the instant 0.7s.

It is presented in Figure 10 the strains of the numerical model. From this image is possible to observe that the column deformation is similar to the predicted in Figure 1 (c).

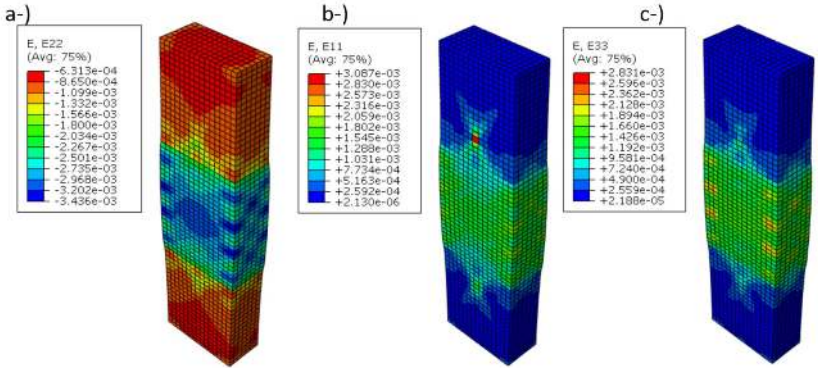

Figure 10 – Strain distributions on the sandwich column: a-) Vertical direction 2; b-) Horizontal direction 1; c-) Horizontal direction 3.

The confinement behavior of the sandwich column can be understood by analyzing the vertical and lateral stresses distribution an instant before rupture. Noting the stress distribution S22 presented in Figure 11, it can be seen that the maximum vertical stresses are located in the corners immediately above and under the slab. The lateral stresses given by the Poisson effect were previously sketched in Figure 3 and Figure 4 and can be confirmed in S11 and S33 distributions (Figure 11b and Figure 11c).

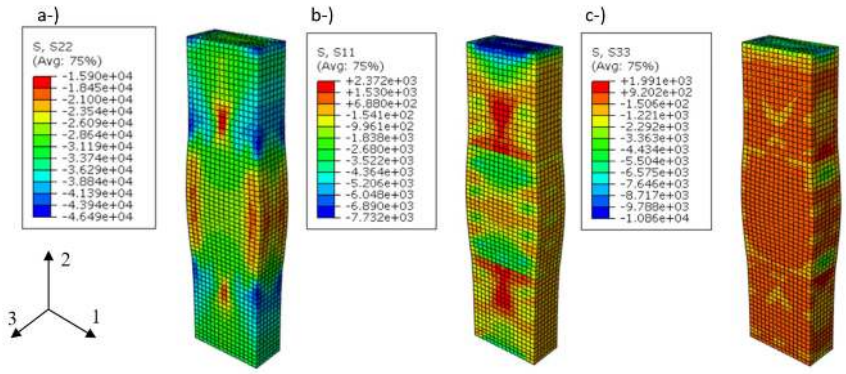

Figure 11 – Stress distributions on the sandwich column (kN/m^2): a-) Vertical direction S22; b-) Horizontal direction S11; c-) Horizontal direction S33.

The lateral stress distributions for different concrete strength ratios and for $h/c = 3.57$ are shown in Figure 12. All models simulated have shown the major lateral stresses in S11 direction, which is the direction of the larger dimension of the column cross section.

The smallest horizontal stress presented on the column should be used to evaluate the confinement of the column, i.e., the stresses in direction 3 governs the confinement. This finding agrees with Ospina and Alexander (1998) and with the Australian concrete code AS 3600 (2018) that recommended the use of the smallest dimension of the column as a parameter c.

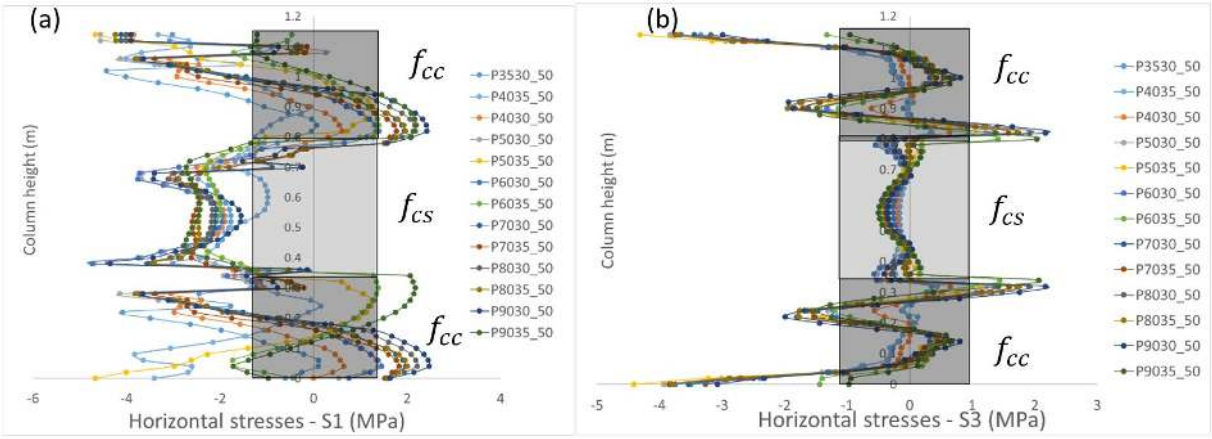

Figure 12 - Lateral stresses along the column height for PS-30 and h/c=3.57. (a) Stresses on direction 1; (b) Stresses on direction 3.

When the concrete strength ratio (f_{cc}/f_{cs}) is under 1.33 and the h/c ratio is greater than 1, the lateral stresses are small and the confinement can be neglect. Therefore, for h/c smaller than 1, even for concrete strengths ratio under 1.33, the lateral stresses are big enough to have confinement in the column.

The damage evolution of sandwich column numerical experiments is illustrated in Figure 13. It is noted that the compressive damage starts at the NSC, f_{cs} (slab) spreading to HSC, f_{cc} region, at the final instant. The tensile damage is located as expected, above and under the lower strength concrete, f_{cs} region. The same behavior was noticed by Shu and Hawkins (1992), Ospina and Alexander (1998), and Choi et al. (2020) in experimental tests.

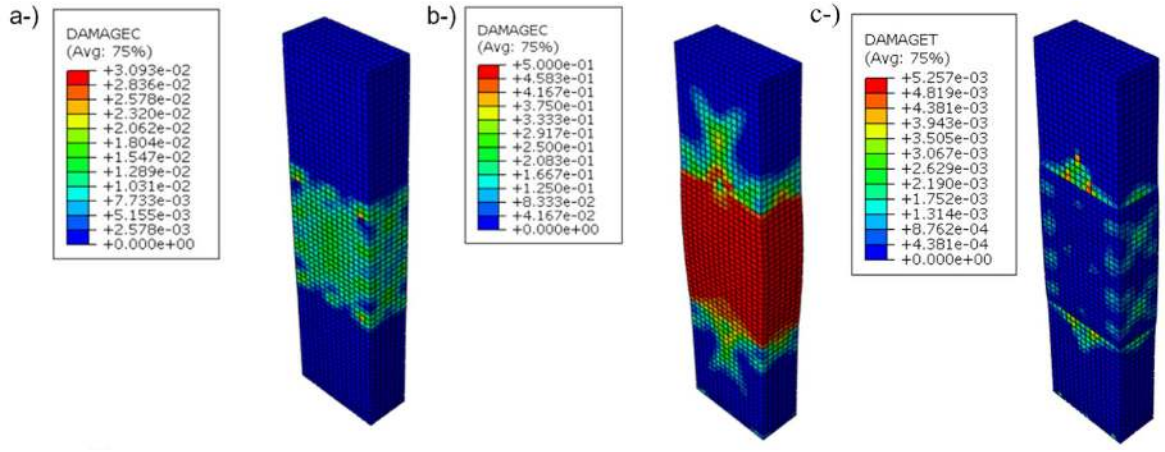

Figure 13 - Compression and tension damage on the column. (a) the instant of initial compression damage. (b) compression damage at the final instant. (c) tensile damage at the final instant.

The numerical results obtained in this study were compared with the effective compressive strength calculated using the expression proposed by Bianchini et al. (1960), Shu and Hawkins (1992), Kayani (1992), Freire (2003), Caporrino (2007) and Shahid (2015) (Figure 14). In Figure 15 were also plotted the design codes curves for effective compressive strength recommended in the ACI 318-19 (2019), CSA23.13 (2014) and the AS3600 (2018).

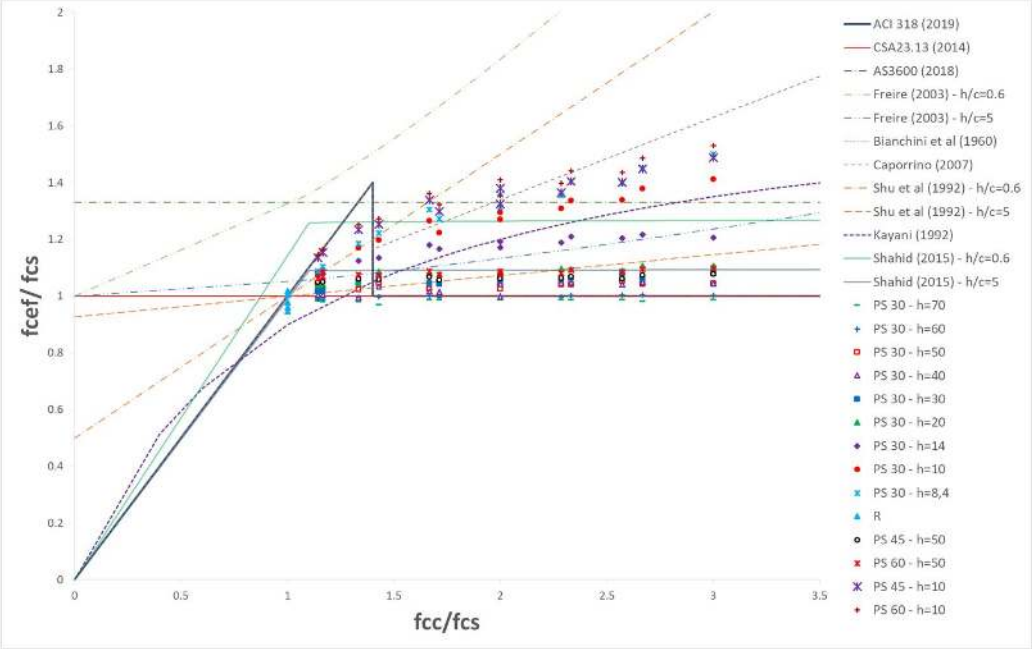

Figure 14 - Numerical results compared to the resistance curves proposed by other authors.

The results presented in Figure 14 shows the importance of considering the h/c ratio as it gives different results. For h/c ratio under 0.71 the numerical results can be well represented by the proposed resistance curves of Kayani (1992), Shahid (2015), and by the standards as ACI 318-19 (2019) and CSA23.13 (2014). However, for h/c ratio above 0.71 only the Canadian standard CSA23.13 (2014) could represent safely the numerical results.

The numerical results were put together with the experimental results of Bianchini, Woods and Kesler (1960); Gamble and Klinar (1991); Shu and Hawkins (1992); Ospina and Alexander (1998); McHarg et al. (2000); Tula et al. (2000); Santos (2004); Lee and Mendis (2004); Caporrino (2007); Meira (2009); Azevedo (2014); Shin et al. (2015) and Choi et al. (2020) presented in Figure 15.

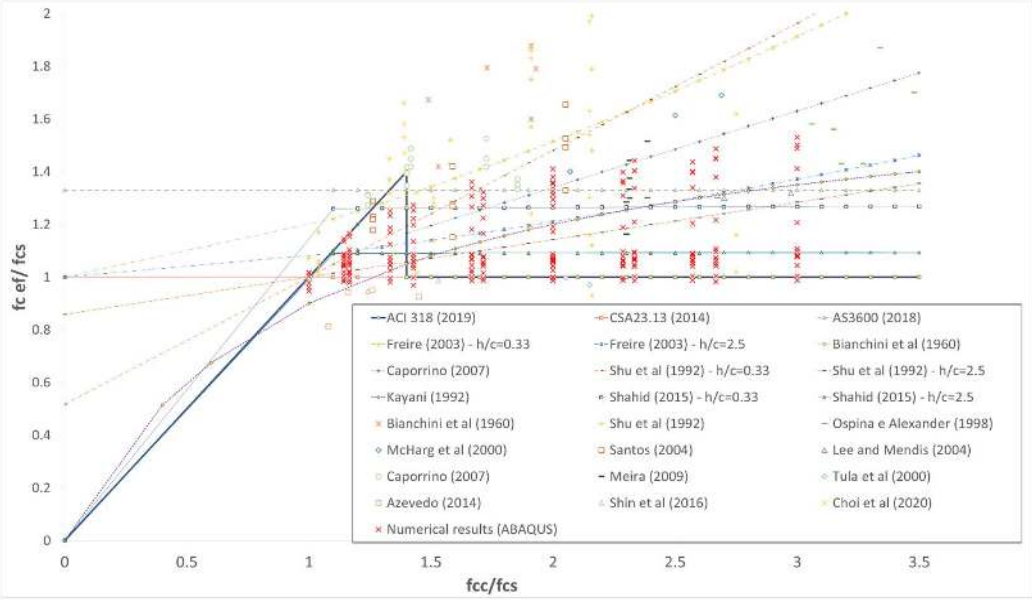

Figure 15 - Numerical and experimental results compared to the curves proposed by other authors.

The experimental results reported by Azevedo (2014) differ from the results provided by any expressions for corner columns. All others results are met by the expression of Shu and Hawkins (1992), Freire (2003), Shahid (2015), and by the standards of ACI 318-19 (2019) and CSA23.13 (2014).

The expression that best fits the tests safely varies according to the relationship between the thickness of the slab and the smallest column width (h/c). For a h/c ratio greater than 1.4 the only expression that meets all cases is that of the Canadian standard (CSA23.13 (2014)). For h/c values under 1.4, the expressions of Kayani (1992) and Shahid (2015) are the ones that best describe them.

For a better estimation on the effective resistance of the sandwich columns it is proposed a calculation method based on the analytical expressions presented in Item 2 with the results of the numerical models.

4 Proposed expression

The proposed expression is based on the numerical estimate of the areas A_{cc} and $A_{cs}$where the lateral stresses are applied to calculate the effective compressive stress. A set of different expressions to calculate the areas A_{cc} and A_{cs} in function of the slab thickness (h) and the dimensions of the column (b, c) is proposed. These expressions were set up based on the stress distribution presented in Figure 3 and Figure 12. It was adopted a parabolic lateral stress distribution at the HSC and a linear distribution at the NSC.

Noting the finite element models, it was realized that both parameters (b, c) that define the cross-section is relevant to estimate areas A_{cs} and A_{cc}. The smaller it is the slab thickness, the larger is the confinement stress, thus, the larger should be the A_{cc} and smaller the A_{cs}. For columns where the ratio is $h/c > 4$ there is no confinement stress at the middle of the slab, then, there is no gain of resistance on the column. For columns with major ratios b/c, smaller confinement stresses were verified, then it was created the parameter N to adjust the results.

The expressions presented next are the ones that best fits the results.

$$for\ \frac{h}{c} \leq 0{,}3\ then \begin{cases} A_{cs} = hc/4N \\ A_{cc} = Nc^2/1{,}5 \end{cases} \tag{32}$$

$$for\ 0{,}3 < \frac{h}{c} < 0{,}6\ then \begin{cases} A_{cs} = hc/2N \\ A_{cc} = Nc^2/4 \end{cases} \tag{33}$$

$$for\ 0{,}6 \leq \frac{h}{c} \leq 1\ then \begin{cases} A_{cs} = hc/1{,}5N \\ A_{cc} = Nc^2/8 \end{cases} \tag{34}$$

$$for\ 1 < \frac{h}{c} \leq 2\ then \begin{cases} A_{cs} = hc/1{,}5N \\ A_{cc} = Nc^2/16 \end{cases} \tag{35}$$

$$for\ 2 < \frac{h}{c} \leq 4\ then \begin{cases} A_{cs} = 1{,}2c^2/N \\ A_{cc} = Nc^2/20 \end{cases} \tag{36}$$

$$for\ \frac{h}{c} > 4\ then\ d\sigma_{cs} = 0\ should\ be\ used \tag{37}$$

Where:

$$for\ \frac{b}{c} \leq 2{,}5\ \rightarrow N = 1 \tag{38}$$

$$for\ 2{,}5 < \frac{b}{c} \leq 3{,}5\ \rightarrow N = 1{,}2 \tag{39}$$

$$for\ 3{,}5 < \frac{b}{c} \leq 4{,}5\ \rightarrow N = 1{,}3 \tag{40}$$

$$for\ \frac{b}{c} > 4{,}5\ \rightarrow N = 1{,}4 \tag{41}$$

The first step is to choose the parameter N in function of b/c ratio. After that, considering the h/c ratio, the area A_{cc} and A_{cs} are estimated. The effective compressive stress is calculated iteratively supposing an initial value for σ_i to calculate the initial lateral stress on the slab ($d\sigma_{cs,i}$). Also, the longitudinal strains in the column (ε_{cc}) and slab (ε_{cs}) are

calculated using equation 19 and 20, respectively. These strains values are replaced into the equation 17 to calculate the lateral stress on the slab ($d\sigma_{cs}$) and then compared with the initial lateral stress from Equation 18. The iterative processes is interrupted when the convergence is reached. The final value of σ_i will be σ_i=$f_{cef} \leq f_{cc}$. These numerical process considered $\alpha = 1$, thus, if α is different, σ_i=f_{cef}/α.

A flowchart of the calculation method is presented on Figure 16 and Figure 17.

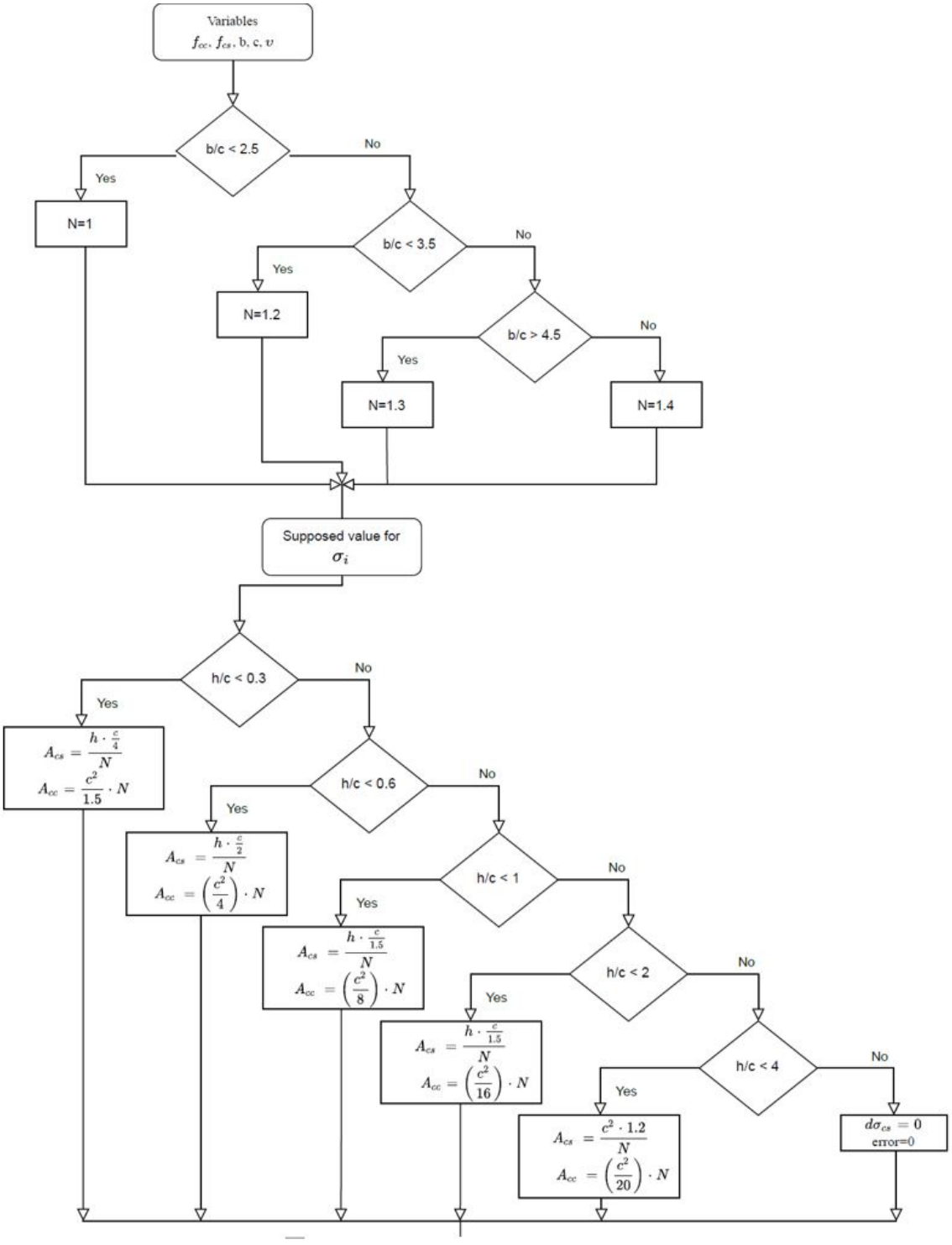

Figure 16 - Part 1 of the flowchart of the proposed model.

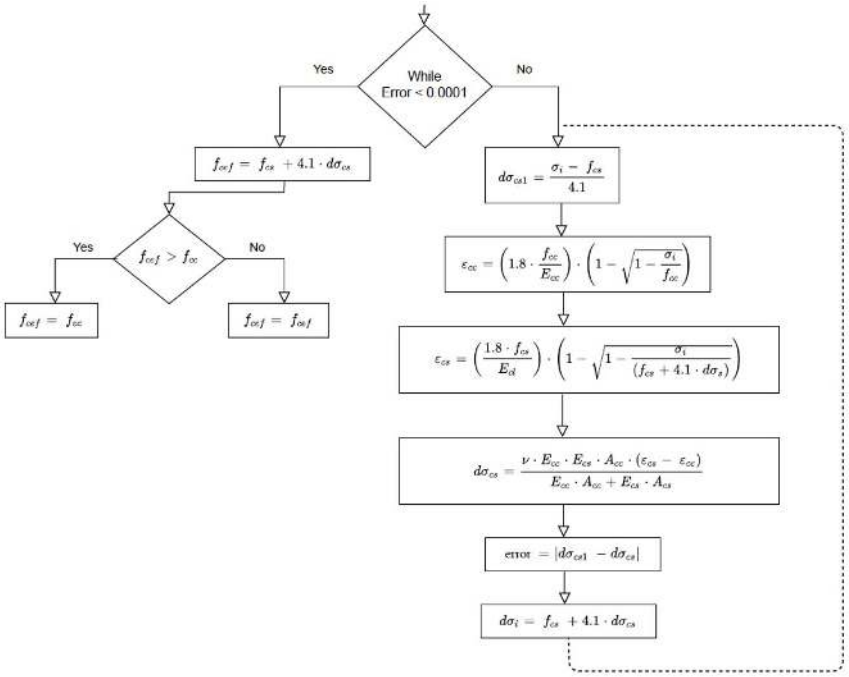

Figure 17 - Part 2 of the flowchart of the proposed model.

The effective compressive strengths obtained with the numerical models were compared with the expression results and shown in Figure 18. In all cases, the results of the proposed expressions agree with the numerical models of the columns, since it was used to calibrate the area A_{cc} and A_{cs} values. The maximum average error found was 2.4% with a standard deviation of 5%.

The expressions were also tested against the experimental results of Shu and Hawkins (1992), Ospina and Alexander (1998), Lee and Mendis (2004) and Choi et al. (2020) (see Figure 19).

The results of the proposed expressions had good agreement with the results of Ospina and Alexander (1998) and Lee and Mendis (2004). The average error was of 2% for both set of tested columns of the cited authors. Comparing to Shu and Hawkins (1992) the average error was of 7%. However, when the concrete strength ratio increased to 5.6, the error was considerable, getting on 86%. This shows that the proposed expression could not represent well concrete strengths ratios above 5 for the experimental tests of Shu and Hawkins (1992), but could represent well the Ospina and Alexander (1998) and Lee and Mendis (2004), even for concrete strength ratios above 6. The proposed expression has an average error of 11% with the experimental results of Choi et al. (2020). The results show that the model can better predict the effective compressive strength of columns for higher concrete strength ratios.

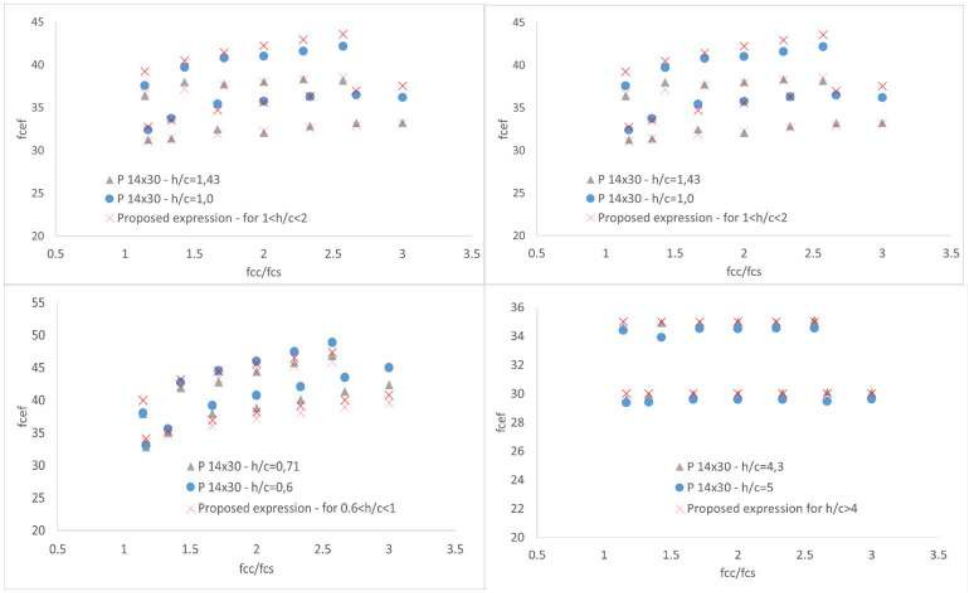

Figure 18 - Numerical results compared with the proposed model.

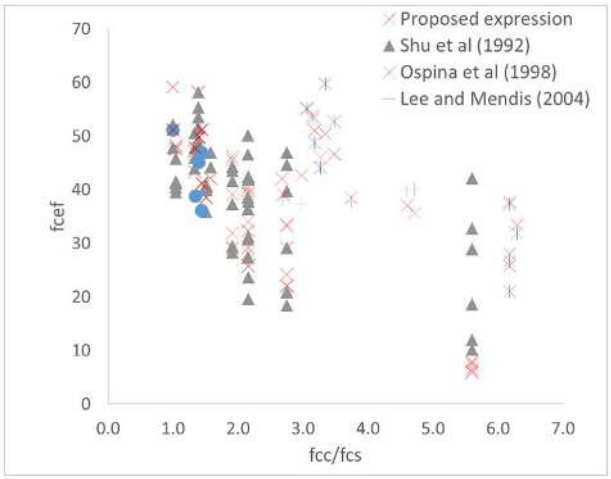

Figure 19 - Experimental results compared with the proposed model.

6 CONCLUSION

In this study, through new nonlinear numerical models, variables that no other author studied have been analyzed and the following conclusions can be drawn from the results and the newly proposed routine for the effective compressive strength of sandwich columns.

- The numerical nonlinear models well represented the experimental results of other authors. The results varied slightly, but the average difference in results was only 3%.
- The analyzes of the horizontal stresses showed that for rectangular cross-section column, the dimension c should be the smallest on the h/c ratio, where the smallest is the ratio, greater is the column resistance. Moreover, it is noted that the b/c ratio had a small influence on the rupture load of the columns.
- The numerical results showed that the parameters with the greatest influence on the stress distribution are the h/c and concrete strengths ratio (f_{cc}/f_{cs}).
- For results of $h/c > 4$ the confining stresses decrease considerably, as predicted on Figure 3a, and it is suggested that only the slab concrete strength should be used on the column resistance.
- The columns with h/c ratio under 1.43 had an effective increase in the column resistance, therefore, it is suggested to use h/c ratios under this value for a better column performance.
- The results showed that the concrete strength ratio is more significant for the f_{cef}/f_{cs} ratio than the concrete strength itself.
- Usually the existence of dowels is necessary for the lap splice of the steel rebars, however for a better confinement behavior of the normal strength concrete, the dowels should be above the slab level.
- For h/c ratio greater than 1.4 the only expression found in the bibliography that is conservative for all cases is the one of the Canadian standard (CSA23.13 (2014)). For h/c values under than 1.4, the expressions of Kayani (1992) and Shahid (2015) are the ones that best describe the results.
- A new prediction model for the effective compressive strength of sandwich columns was developed. This proposed model had good agreement with the numerical and experimental results, presenting a mean error of 2.4% and 3.7%, respectively.

Author Contributions: Conceptualization, FS Prado, FR Stucchi and LC Meneghetti; Methodology, FS Prado; Investigation, FS Prado; Writing - original draft, FS Prado, LC Meneghetti; Writing - review & editing, FR Stucchi and LC Meneghetti; Resources, FR Stucchi and LC Meneghetti; Supervision, LC Meneghetti.

Editor: Marco L. Bittencourt.

References

ALI SHAH, S.A.; RIBAKOV, Y. (2005). Experimental and analytical study of flat-plate floor confinement. Elsevier: Materials and Design, p. 655-669.

ALI SHAH, S.A.; RIBAKOV, Y. (2008). Using mechanics of materials approach for calculating interior slab-column joints strength. Elsevier: Materials and Design, p. 1145-1158.

ALI SHAH, S.A.; RIBAKOV, Y. (2011). Estimation of RC slab-column joints effective strength using neural networks. Latin American Journal of Solids and Structures, p. 393-411.

AMERICAN CONCRETE INSTITUTE. (1963). ACI 318-63: building code requirements for reinforced concrete and commentary. Farmington Hills, Mich.

AMERICAN CONCRETE INSTITUTE. (2019). ACI 318-19: building code requirements for reinforced concrete and commentary. Farmington Hills, Mich.

Associação Brasileira de Normas Técnicas. (2014) NBR-6118: projeto de estruturas de concreto – procedimentos. Rio de Janeiro.

AUSTRALIAN STANDARDS. (2018). AS 3600: Concrete Structures. Sydney.

AZEVEDO, P.R. (2014). Confinamento dado por vigas e lajes a pilares feitos com concretos de diferentes resistências ao longo da altura. 167 p. Dissertação. Escola Politécnica, Universidade de São Paulo, São Paulo.

BIANCHINI, A. C.; WOODS, R. E.; E. KESLER, C. E. (1960). Effect of floor concrete strength on column strength. ACI Journal, Proceedings. v. 31, n. 11, p. 1149-1169.

BIRTEL, V.; MARK, P., BOCHUM R. (2006). Parameterized Finite Element Modelling of RC Beam Shear Failure. ABAQUS User's Conference, p. 95-108.

CANADIAN STANDARDS ASSOCIATION. (2014). CSA A23.3-14: design of concrete structures. Mississauaga, Ontario.

CAPORRINO, C.F. (2007). Confinamento dado por lajes e vigas melhorando a resistência do pilar que as cruza. 125 p. Dissertação (Mestrado). Escola Politécnica, Universidade de São Paulo, São Paulo.

CHOI, S. H.; LEE, D. H.; HWANG, J. H.; OH, J. Y.; KIM, K. S.; KIM, S. H. (2018). Effective compressive strengths of corner and exterior concrete columns intersected by slabs with different compressive strengths. Archives of Civil and Mechanical Engineering, v. 18, n. 3, 2018, p. 731–741.

CHOI, S. H.; LEE, D. H.; HWANG, J. H.; HAN, S. J.; CHO, H. C.; KIM, K. S.; KIM, S. H. (2020). Simplified Effective Compressive Strengths of Columns with Intervening Floor Slabs. International journal of concrete. Structures and Materials. v. 14, n. 1, p. 1–11.

Dassault Systèmes. (2014). ABAQUS Analysis User's Manual v.6-14. Providence, USA.

DRUCKER, D. C.; PRAGER, W. (1952). Soil mechanics and plastic analysis ou limit design. JSTOR, Brown university. v. 10, n. 2, p. 157–165.

FÉDÉRATION INTERNATIONALE DU BÉTON. (2013). fib Model Code for Concrete Structures 2010. p. 432, Ernst and Sohn. Berlim.

FREIRE, L. (2003). Resistência de pilares de concreto de alta resistência interceptados por elementos de concreto de menor resistência. 2003. 119 p. Dissertação (Mestrado) – COPPE, Universidade federal do Rio de Janeiro, Rio de Janeiro.

GAMBLE, W.L.; KLINAR, J.D. (1991). Tests of high-strength concrete columns with intervening floor slabs. ASCE: Journal of Structural Engineer, v. 5, n. 117, p. 1462-1476.

GUIDOTTI, R.; RUIZ, M.F.; MUTTONI, A. (2011). Crushing and flexural strength of slab-column joints. Elsevier: Engineering Structures, p. 855-867.

Hsu, T T. C.; Zhang, Li-Xin. (1996). Tension Stiffening in Reinforced Concrete Membrane Elements. Structural Journal. v. 93, n.1, p. 108-115.

KAMINSKI, M.; KMIECIK, P. (2011). Modelling of reinforced concrete structures and composite structures with concrete strength degradation taken into consideration. Archives of Civil and Mechanical Engineering, v. 11, n. 3, p. 623-636.

KAYANI, M.K.R. (2000). Load transfer from high strength concrete columns though lower strength concrete slabs. Thesis. University of Illinois, Urbana, Illinois.

LEE, S. C.; MENDIS, P. (2004). Behavior of High-Strength Concrete Corner Columns Intersected by Weaker Slabs with Different Thicknesses. ACI Structural Journal, v. 101, n. 1, p. 11–18.

F.; ALFARAHN; LÓPES-ALMANSA, F.; OLLER, S. (2017). New methodology for calculating damage variables evolution in Plastic Damage Model for RC structures. Engineering Structures, v. 132, p. 70-86.

LEE, J.; FENVES, G.L. (1998). Plastic-damage model for cyclic loading of concrete structures, Journal of engineering mechanics, v. 124, n. 8, p. 892-900.

LUBLINER, J.; OLIVER, J.; OLLER, S.; ONATE, E. (1989). A plastic-damage model for concrete, Int. J. Solids Structures, v. 25, n. 3, p. 299-326.

MAEKAWA, A.; PIMANMAS, A.; OKAMURA, H. (2004). Nonlinear mechanics of reinforced concrete. Taylor and Francis Group.

MALM, R. Predicting shear type crack initiation and growth in concrete with nolinear finite element method. (2009). Tese (Doutorado) – Royal Institute of Technology (KTH), Estocolmo.

MCHARG, P.J.; Cook W. D.; Mitchell D.; Y. S. Yoon. (2000). Improved transmission of high-strength concrete column loads through normal strength concrete slabs. ACI Structural Journal, n. 97-S18, p. 149-157.

MEIRA, M. (2009). Estudo experimental de ligações pilares-vigas de concreto de diferentes resistências. 267 p. Tese (Doutorado) – Pontifícia Universidade Católica do Rio de Janeiro, Rio de Janeiro.

OSPINA, C.E.; ALEXANDER, S.D.B. (1998). Transmission of interior concrete column loads through floors. ASCE: Journal of Structural Engineering, v. 124, n. 6, p. 602-610.

RICHART, F.E.; BROWN, R.L., (1934). An Investigation of Reinforced Columns, University of Illinois Engineering Experiment Station Bulletin n. 267. University of Illinois, Urbana, p. 91.

SANTOS, A.P.S. (2004). Análise do confinamento dado por lajes em pilares com concretos de diferentes resistências ao longo da altura. 2004. 110 p. Dissertação (Mestrado) – Escola Politécnica, Universidade de São Paulo, São Paulo.

Shah, Abid A Dietz, Joerg Tue, Nguyen V Koenig, Gert. (2005). Experimental Investigation of Column-Slab Joints. n. 102, p. 103–113.

SHAHID, I.; Farooq, S. H.; Qureshi, N. A.; Kayani, K. R.; Mumtaz, H. (2015). Effective Concrete Strength within Slab- Column Joint. v. 7, n. 3, p. 965–972.

SHIN, H. O.; YOON, Y. S.; COOK, W.D.; MITCHELL, D. (2015). Effect of Confinement on the Axial Load Response of Ultrahigh-Strength Concrete Columns, Journal of Structural Engineering, v. 141, n. 6, p. 04014151- 040141512.

SHIN, H. O.; YOON, Y. S.; MITCHELL, D., (2017). Axial load transfer in non-slender ultra-high-strength concrete columns through normal-strength concrete floor slabs, Journal of Structural Engineering, v. 136, p. 466-480.

SHU, C.; HAWKINS, N.M. (1992). Behavior of columns continuous through concrete floors, ACI Structural Journal, v. 89, n. 4, p. 405-414.

TULA, L.; HELENE, P; DIAZ, N; BORTOLUCCI, A. (2000). Resistência à compressão do concreto confinado.: Congresso Brasileiro do Concreto, 42º, 2000, Fortaleza. Anais. IBRACON, Fortaleza.

Urban, T. S., & Gołdyn, M. M. (2015). Behaviour of eccentrically loaded high- strength concrete columns intersected by lower-strength concrete slabs. Structural Concrete, 16(4), 480–495.